

Engineering the quantum transport of atomic wavefunctions over macroscopic distances

A. Alberti, V. V. Ivanov, G. M. Tino and G. Ferrari
*Dipartimento di Fisica and LENS - Università di Firenze, CNR-INFN,
 INFN - Sezione di Firenze, via Sansone 1, 50019 Sesto Fiorentino, Italy*

PACS numbers:

The manipulation of matter waves represents a milestone in the history of quantum mechanics. The first experimental validation of matter wave behavior occurred with the observation of diffraction of matter by crystals[1], and then with grating and Young's double-slit interference with electrons, neutron, atoms and molecules [2, 3, 4, 5]. More recently matter wave manipulation has become a building block for quantum devices such as quantum sensors [6] and it plays an essential role in many proposals for implementing quantum computers [7, 8]. In this letter we demonstrate coherent control of the spatial extent of an atomic wavefunction by reversibly stretching and shrinking the wavefunction over a distance of more than one millimeter. The remarkable experimental simplicity of the scheme could ease applications in the field of quantum transport and quantum computing.

Ultracold atomic gases trapped in optical lattices (large and periodic ensembles of optical microtraps created by interfering optical laser beams) provide ideal tools for studying quantum transport in different regimes [9, 10] and quantum many body systems in periodic potentials [11, 12, 13, 14]. One of the challenges in this field is to coherently transfer matter waves between macroscopically separated sites. This would provide a mechanism to couple distant quantum bits and ultimately would lead to quantum information processing with cold atoms in optical lattices [15]. Recently it was demonstrated that spatially driven lattice potentials in the presence of a linear potential can induce a coherent delocalization of a matter wave [16] when the driving is applied at a frequency equivalent to the Bloch frequency ν_B , i.e., the linear potential between adjacent sites expressed in frequency units. The delocalization occurs at integer multiples of ν_B because of the resonant coupling between Wannier-Stark levels within the same band. The resonances are characterized by a $\text{sinc}(2\pi t\Delta\nu)$ spectral profile, where t is the driving time and $\Delta\nu$ is the detuning of the driving from the resonant frequency. The sinc response here arises from the influence on the tunneling current of the relative phase ϕ between the driving and the site-to-site quantum phase in the broadened wavefunction. When ϕ lies between 0 and π the wavefunction expands, while when it lies between π and 2π the wavefunction shrinks. In particular when $\phi = 2\pi$ the wavefunction returns to the starting point. Such a reversible behavior is expected provided that the evolution of the wavefunction is fully coherent.

Any mechanism introducing loss of coherence would

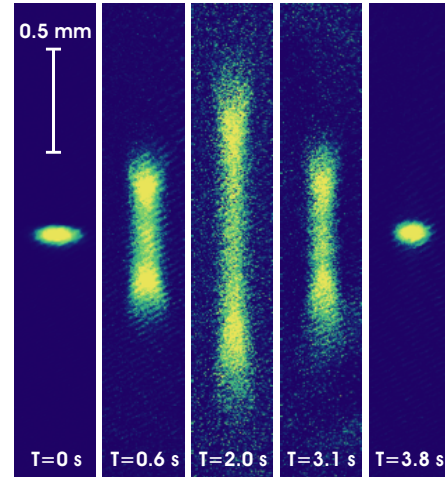


Figure 1: Revivals of the spatial distribution of the atoms in the lattice potential under strong, non-resonant driving with an amplitude of 10 lattice sites peak-to-peak. In the picture the lattice is vertically aligned and the driving is active for times ranging from 0 to 3.8 seconds. The frequency detuning of the driving δ is set to about 250 mHz, which results in a revival time of 3.8 seconds. At $T=0$ the *in-situ* RMS spatial width is $31 \mu\text{m}$, while at $T=3.8$ s it becomes $40 \mu\text{m}$. The color scale is adapted to each picture so that visibility is maintained with the varying atomic densities.

in fact lead to a non-reversible broadening. However, in a decoherence free regime, it should be possible to engineer the spatial extension of the wavefunction using the frequency offset and amplitude of the driving as tuning knobs. Here we experimentally demonstrate this new technique of matter wave manipulation by showing that coherent delocalization results in an extended distribution corresponding to the size of the broadened wavefunction. This is demonstrated by observing *in-situ* the breathing of the wavefunction under non resonant driving conditions, and through a self interference technique based on time-of-flight expansion. Our experimental findings are supported by a theoretical model with which, using the basis of Wannier-Stark eigenstates of the static Hamiltonian, we can determine analytically the spatial wavefunction under the action of the driving.

In order to drive (i.e., modulate) the phase of the lattice potential, we apply a sinusoidal voltage (with frequency ν_{PZT}) to the piezo-electric transducer (PZT) that

supports the retro-reflecting mirror of the optical dipole standing-wave. In a first set of measurements we test the spatial coherence of the broadened wavefunction by observing the periodic breathing of the atomic distribution while we drive the PZT with a non-zero frequency detuning $\Delta\nu = \nu_{\text{PZT}} - \nu_B$. Fig. 1 displays the image of the atomic distribution under hard driving conditions. The frequency detuning $\Delta\nu$ is set to about 0.26 Hz such that revival period is about 4 seconds and the amplitude of the driving is set to its maximally experimentally accessible value, ten lattice sites peak-to-peak. The spatial profile is initially gaussian, corresponding to how the atoms are loaded into the lattice potential. The profile then evolves into a more complex shape as a result of the wavefunction broadening [18, 19], but then at the revival the distribution returns to its initial profile. Starting from a size of 31 μm it reaches an extension larger than 1.5 mm, and then it returns to a size of 40 μm . In other words, the distribution increases its size by a factor larger than 20 and then returns to almost to its initial value [20]. Intermediate values of the spatial extent can be obtained in a reproducible and reversible way by varying the amplitude or frequency detuning $\Delta\nu$ of the driving voltage.

In Fig. 2 we show the time evolution of the spatial extent for different values of frequency detuning $\Delta\nu$. In Fig. 2a and b, with $\Delta\nu$ equal to +5 Hz and -5 Hz respectively, the breathing shows a revival with the expected period of 5 Hz, and a constant visibility on a one second timescale, regardless of the sign of the frequency detuning. Fig. 2c is similar to Fig. 2a but with $\Delta\nu = 0.5$ Hz. Again the atomic distribution shows a breathing at a frequency equal to $\Delta\nu$, and from the reduction of the oscillation amplitude over time we can infer a e^{-1} damping time of 28 seconds. The results presented in Fig. 1 and 2 can not be explained classically and show a quantitative agreement with the analytic expression of the wavefunction expected for the driven potential [18, 19, 20]. This implies that we manipulate, and directly observe, the spatial wavefunction on a length scale larger than 1 mm.

To study the coherence properties of the modified wavefunction we measure the interference of the wavefunction with itself. To this end, the wavefunction is expanded in time-of-flight (TOF) after an adiabatic release from the lattice potential. We record the evolution for the interval between 0 to 25 ms under various driving conditions. First we consider the momentum distribution under resonant driving (i.e., $\Delta\nu = 0$). An integer number of sinusoidal cycles, up to 120 (equivalent to 210 ms when $\nu_B = 574.14$ Hz), is applied to the PZT such that the wavefunction broadens proportionally with time. The momentum distribution then is probed in TOF 300 ms after the beginning of the driving, and after switching off the lattice potential adiabatically on a 20 μs timescale. Fig. 3 shows the changes in the expansion after 15 ms of TOF for various broadening conditions. In the absence of a driving voltage, the thermal sample expands as expected yielding a gaussian profile. When we drive the system, we clearly observe the appearance of a non-

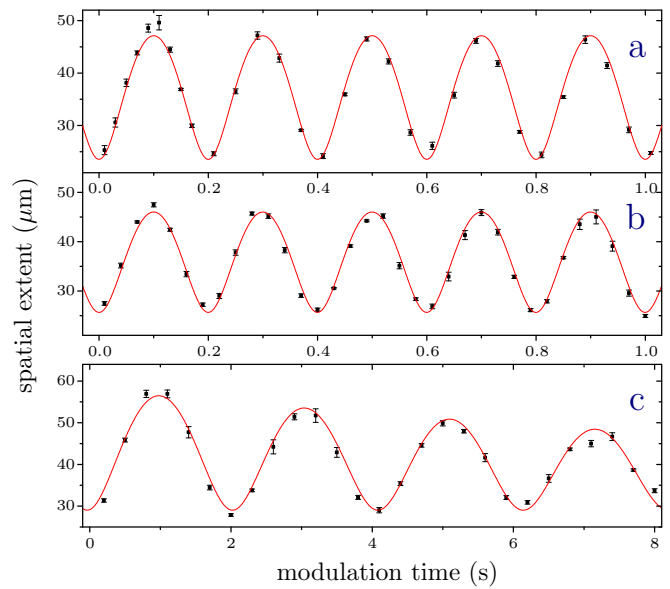


Figure 2: Dynamics and revivals of the atomic extent under non-resonant driving of the lattice phase. For short times the minimum size corresponds to the size of the non-driven atomic cloud. a) detuning $\delta = \nu_{\text{PZT}} - \nu_B = +5$ Hz, b) $\delta = -5$ Hz, c) $\delta = -0.5$ Hz. The driving amplitude is set to about 1 (a and b) and 0.2 (c) lattice sites peak-to-peak. From the data in c) we infer a e^{-1} damping time of 28 s. In each graph the fitted line gives, within the error bars, a periodicity equal to δ^{-1} .

Gaussian distribution. Here we can distinguish two components: the first is directly related to the expansion in absence of the modulation, while the second one has a spatial extent and relative weight related to the broadening. This results from the interference among the probability amplitude originating from the different portions of the wavefunction as directly checked by a simulation of the ballistic expansion of the broadened wavefunction. As expected, when the free expansion due to the momentum dispersion is of the order of the size of the broadened wavefunction, the interference pattern reaches maximum visibility.

There is an additional effect that, in principle, can complicate the observed TOF profiles. For a static lattice (i.e., one without a driving force applied to the PZT) the position of the interference peak exhibits periodic dynamics at the Bloch frequency ν_B . This result, shown in Fig. 4, reflects the time evolution of the site-to-site phase differences in the wavefunction and is confirmed by simulation of the wavefunction expansion. This phenomenon is in direct analogy with Bloch oscillations where the atoms, subject simultaneously to a constant force (i.e., gravity in this case) and the lattice potential, sweep periodically the first Brillouin zone [17]. In the TOF images this is observed as an increase of the momentum of the interference peak linearly in time, until it reaches the lattice photon recoil and changes sign. At this point the

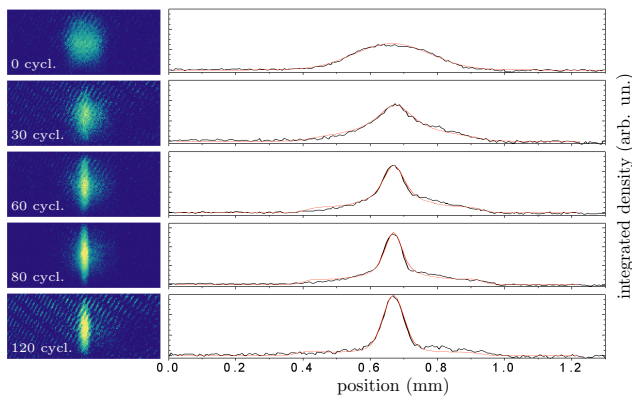


Figure 3: Effect of the driving on the ballistic expansion of the sample. The time-of-flight is fixed to 15 ms and a resonant driving is applied during a fixed amount of cycles. Left side: 2D density profile. In the pictures the vertical gravity and the lattice are horizontally oriented. Right side: the atomic density integrated along the transverse direction of the lattice. The red line is the distribution expected from the ballistic expansion of the analytical expression of the broadened wavefunction [21]. Both the colour scale on the 2D distribution and the vertical scale on the integrated density profiles are the same for the various driving conditions.

interference peak is split in two parts. In order to simplify the treatment and neglect this additional effect, the pictures of Fig. 3 and the subsequent analysis are made by starting the TOF at point where the interference peak has maximum amplitude or, equivalently, it is centered in the first band before the release from the lattice.

We have confirmed both the appearance of the interference pattern and its Bloch like dynamics by simulating the evolution in the static lattice and the free expansion of the analytic form of the broadened wavefunction [18]:

$$|n(t)\rangle = \sum_{n'=-\infty}^{+\infty} e^{-in'2\pi\nu_B t} e^{i\pi(n-n')\Delta\nu t} \times J_{n-n'}\left(\sin(\pi\Delta\nu t)\frac{2\Omega}{\pi\Delta\nu}\right) |n'\rangle \quad (1)$$

where $|n'\rangle$ are the Wannier-Stark eigentates of the static Hamiltonian (with the gravity potential and the non-modulated lattice) labelled by the index n' of their position expressed in lattice units, $|n(t)\rangle$ is wavefunction of the state $|n\rangle$ subject to the driving during a time t , Ω is a coefficient accounting for the tunneling rate among the lattice barriers, and J_n are the Bessel functions of the first kind. The hypothesis that the initial state corresponds to the Wannier-Stark eigenstate $|n\rangle$ is justified by the fact that the trapped atoms are derived from a thermal sample at a temperature higher than the recoil temperature and they uniformly fill the first band (see the Methods section). The thermal de Broglie wavelength is shorter than the lattice period, so when we load

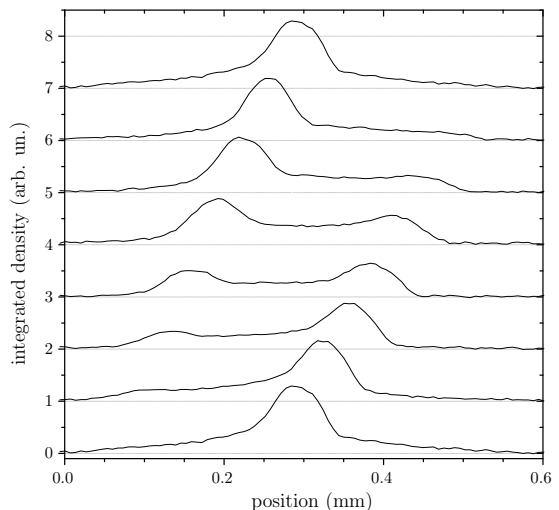


Figure 4: Temporal evolution of the broadened wavefunction phase in the absence of a driving field. In a static potential the combined effect of the lattice and gravity induces a linear increase of the site-to-site phase in the broadened wavefunction. This is observable in the ballistic expansion signal as a periodic evolution of the interference peak for a fixed time-of-flight duration of 15 ms. From top to bottom the trapping time is linearly increased over one Bloch period (about 1.75 ms).

the atoms into the lattice potential, the coherence properties among adjacent Wannier-Stark eigenstates can be neglected. In Fig. 3 the density profiles we derive from the analytical model are in remarkable agreement with the experimental data. It is also worth noting that the Bloch-like dynamics observed in Fig. 4 results only from the long range coherence of the broadened wavefunction. In the absence of driving, on the other hand, the shape of the distribution after ballistic expansion does not show any periodicity.

As an additional check of the agreement between the experiment and theory we verified that the modified distributions in the time-of-flight profiles do not result from a simple selection of a given momentum class. For instance, for the conditions of Fig. 3 the overall atom number does not change with the number of applied cycles; the atomic distribution in this case shifts to the central peak owing to the constructive interference between probability amplitudes from symmetric regions of the wavefunction. In addition, we verified that the wavefunction also exhibits revivals in the interference pattern for the TOF distribution under non-resonant driving. In Fig. 5 we compare the TOF profiles taken for different expansion times under three different conditions: without driving, at maximum expansion, and at the spatial revival. The driving conditions for the last condition are similar to those of Fig. 3 except that the frequency detuning δ is set to about 2 Hz and the driving lasts longer in order to reach a maximum broadening as in Fig. 3 with 80 cycles. The TOF expansion at maximum broadening

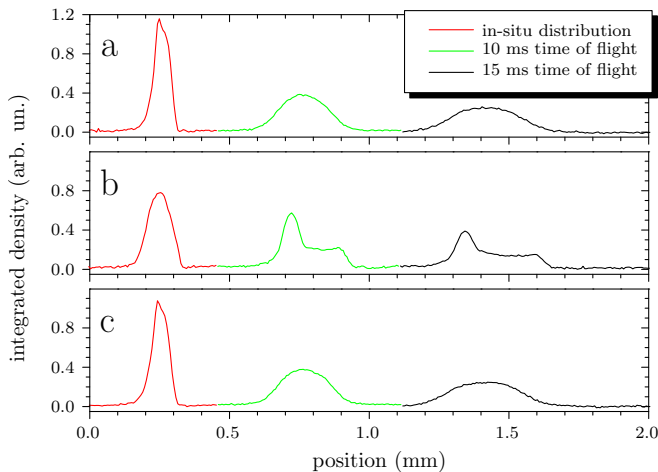


Figure 5: Ballistic expansion under non-resonant driving. The periodic dynamics of the spatial extent have their counterpart in the ballistic expansion signal. From left to right: *in-situ* distribution, 10 ms and 15 ms time-of-flight. A: no driving. B: maximum expansion. C: first spatial revival. In B the driving conditions are the same as those in Fig. 3 for 80 cycles, except here we use a 2.28 Hz frequency detuning of the driving field with respect to the Bloch frequency. The horizontal displacement corresponds to the free fall in the earth gravity field.

is equivalent to that obtained under resonant driving except that now the distribution is deliberately asymmetric because of the different Bloch phase at the release (same as in fig. 4 case 5). On the other hand, the TOF expansion at the time when the distribution shrinks to the initial size, is the same as that in absence of driving.

In summary, we experimentally demonstrate a new method to manipulate the spatial wavefunction of cold strontium atoms over distances of the order of a millimeter. This manipulation preserves the quantum coherence and we find that the process is fully deterministic, reversible, and in quantitative agreement with an analytical model. The controlled stretching and shrinking of the wavefunctions may be applied for implementing new classes of quantum logic gates for q-bits such as

neutral atoms in an optical lattice [22, 23]. It is worth mentioning that neutral atom optical clocks can operate with atoms in conditions similar to those presented in this work [24, 25]. Finally, with stretched wavefunctions we observe a striking dependence of the distribution in ballistic expansion due to site-to-site phase gradients induced by external forces, regardless of the initial temperature of the sample. This approach may find applications in the realization of precise force sensors based on atoms otherwise difficult to cool.

I. METHODS

Experimental setup and procedure

The experimental setup was described previously in [26]. About 10^6 ^{88}Sr atoms are laser cooled to a temperature of $1\ \mu\text{K}$ and subsequently are loaded into a vertical lattice potential produced by the dipole force of a $\lambda_L = 532\ \text{nm}$ laser field. The lattice is formed by retro-reflecting 532 nm laser light with a mirror mounted on top of a piezo-electric transducer (PZT). The phase of the optical lattice, defined to be zero at the surface of the mirror, is modulated by applying a time-dependent voltage to the PZT with a maximum excursion of 10 lattice sites peak-to-peak. The depth of the lattice potential is typically 8 recoil energies E_R ($E_R = h^2/2m\lambda_L^2 = k_B \times 381\ \text{nK}$) along the optical axis of the trapping beam and, in the radial direction, it decreases exponentially due to the gaussian spatial profile. Since initially the atoms are hot with respect to the recoil temperature, when they are loaded into the lattice potential they occupy almost uniformly the first band and, with decreasing weight, the higher bands. Taking into account the full three dimensional lattice potential and including the gravity force, all the bands except the first one have a lifetime shorter than 100 ms. We finish the atom sample preparation sequence by taking advantage of this property to select atoms in the first band, simply by holding the atoms in the static potential for a time of 100 ms. The atomic distribution is measured by absorption imaging of a resonant laser beam detected on a CCD camera.

-
- [1] C. Davisson & Germer, L. H. The scattering of electron by a single crystal of nickel. *Nature* **119**, 558 (1927).
 - [2] Joensson, C. Elektroneninterferenzen an mehreren künstlich hergestellter feinspalten. *Zeitschrift fuer Physik* **161**, 454–474 (1961).
 - [3] Zeilinger, A., Gahler, R., Shull, C. G., Treimer, W. & Mampe, W. Single and double slit diffraction of neutrons. *Reviews of Modern Physics* **60**, 1067–1073 (1988).
 - [4] Carnal, O. & Mlynek, J. Young’s double-slit experiment with atoms: a simple atom interferometer. *Phys. Rev. Lett.* **66**, 2689 (1991).
 - [5] Arndt, M. *et al.* Wave-particle duality of C_{60} molecules. *Nature* **401**, 680–682 (1999).
 - [6] Peters, A., Chung, K. Y. & Chu, S. Measurement of gravitational acceleration by dropping atoms. *Nature* **400**, 849 (1999).
 - [7] Monroe, C., Meekhof, D., King, B. & Wineland, D. A ‘Schrodinger cat’ superposition state of an atom. *Science* **272**, 1131 (1996).
 - [8] Monroe, C. Quantum information processing with atoms and photons. *Nature* **416**, 238 (2002).
 - [9] Madison, K. W., Fischer, M. C., Diener, R. B., Niu, Q. & Raizen, M. G. Dynamical Bloch band suppression in an optical lattice. *Phys. Rev. Lett.* **81**, 5093 (1998).

- [10] Browaeys, A., Haeffner, H., McKenzie, c., Rolston, S. L., Helmerson, K. & Phillips, W. D. Transport of atoms in a quantum conveyor belt. *Phys. Rev. A* **72**, 053605 (2005).
- [11] Bloch, I. Ultracold quantum gases in optical lattices. *Nat. Phys.* **1**, 253001 (2005), and references therein.
- [12] Gemelke, N., Sarajlic, E., Bidet, Y., Hong, S. & Chu, S. Parametric amplification of matter waves in periodically translated optical lattices. *Phys. Rev. Lett.* **95**, 170404 (2005).
- [13] Sias, C. *et al.* Resonantly enhanced tunnelling of Bose-Einstein condensates in periodic potentials. *Phys. Rev. Lett.* **98**, 120403 (2007).
- [14] Sias, C. *et al.* Observation of Photon-Assisted Tunneling in Optical Lattices. *Phys. Rev. Lett.* **100**, 040404 (2008).
- [15] Bloch, I. Quantum coherence and entanglement with ultracold atoms in optical lattices. *Nature* **453**, 1016 (2008), and references therein.
- [16] Ivanov, V. V. *et al.* Coherent delocalization of atomic wave packets in driven lattice potentials. *Phys. Rev. Lett.* **100**, 043602 (2008). Unlike the present work, in the reference we study the spectral properties of the "delocalization" resonances and we show that they are Fourier limited with respect to the duration of the driving.
- [17] Dahan, M. B., Peik, E., Reichel, J., Castin, Y. & Salomon, C. Bloch oscillations of atoms in an optical potential. *Phys. Rev. Lett.* **76**, 4508 (1996).
- [18] Thommen, Q., Garreau, J. C. & Zehnlé, V. Quantum interference in a driven washboard potential. *Am. J. Phys.* **72**, 1017 (2004).
- [19] Thommen, Q., Garreau, J. C. & Zehnlé, V. Atomic motion in tilted optical lattices: an analytical approach. *J. Opt. B: Quantum Semiclass. Opt.* **6**, 301 (2004).
- [20] The non complete reversibility of the quantum process observed in Figs. 1 and 2 results from technical, rather than fundamental, limits of the experimental demonstration. Namely the stability of the vertical alignment of the lattice potential affects the definition of the ν_B which, in turns, determines the instant of exact refocussing of the distribution with increasing sensitivity at longer times. This effect, combined to the chosen fast tunnelling rate, accounts for the non exact refocussing of the distribution in observed in Fig. 1. The decoherence measured in Fig. 2 is attributed to the off resonant scattering of the trapping photons.
- [21] The theoretical profile is calculated numerically applying the free particle Hamiltonian to the wavefunction of eq. 1 using the double Fourier transform method. According to the notation of eq. 1 the theoretical profiles are calculated supposing $\Delta\nu = 0$ and $2\Omega t = \text{number of cycles} \times 1.5$. The latter condition is consistent with the tunneling rate calculated from the overlap of adjacent Wannier-Stark eigenstates [18] considering the experimental conditions. The calculation of the theoretical profiles includes also the convolution with the initial distribution.
- [22] Hayes, D., Julienne, P. S. & Deutsch, I. H. Quantum logic via the exchange blockade in ultracold collisions. *Phys. Rev. Lett.* **98**, 070501 (2007).
- [23] Creffield, C. E. Quantum Control and Entanglement using Periodic Driving Fields. *Phys. Rev. Lett.* **99**, 110501 (2007).
- [24] Takamoto, M., Hong, F.-L., Higashi, R. & Katori, H. An optical lattice clock. *Nature* **435**, 321 (2005).
- [25] Ludlow, A. D. *et al.* Sr lattice clock at 1×10^{-16} fractional uncertainty by remote optical evaluation with a Ca clock. *Science Express* DOI: 10.1126/science.1153341, (2008).
- [26] Ferrari, G., Poli, N., Sorrentino, F. & Tino, G. M. Long-lived Bloch oscillations with bosonic Sr atoms and application to gravity measurement at the micrometer scale. *Phys. Rev. Lett.* **97**, 060402 (2006).

Acknowledgements We would like to thank M. Artoni, N. Poli, C. W. Oates and M. L. Chiofalo for stimulating discussions, M. Schioppo for his contribution in the early stage of the experiment, and R. Ballerini, M. De Pas, M. Giuntini, A. Hajeb, and A. Montori for technical assistance. This work was supported by LENS, INFN, EU (under Contract No. RII3-CT-2003 506350 and the FINAQS project), ASI and Ente CRF.

Competing Interests The authors declare that they have no competing financial interests.

Correspondence Correspondence and requests for materials should be addressed to G.F. (email: ferrari@lens.unifi.it).